2D MATERIALS

Tuning electron correlation in magic-angle twisted bilayer graphene using Coulomb screening

Xiaoxue Liu[1], Zhi Wang[1], K. Watanabe[2], T. Taniguchi[2], Oskar Vafek[3,4], J. I. A. Li[1]*

Controlling the strength of interactions is essential for studying quantum phenomena emerging in systems of correlated fermions. We introduce a device geometry whereby magic-angle twisted bilayer graphene is placed in close proximity to a Bernal bilayer graphene, separated by a 3-nanometer-thick barrier. By using charge screening from the Bernal bilayer, the strength of electron-electron Coulomb interaction within the twisted bilayer can be continuously tuned. Transport measurements show that tuning Coulomb screening has opposite effects on the insulating and superconducting states: As Coulomb interaction is weakened by screening, the insulating states become less robust, whereas the stability of superconductivity at the optimal doping is enhanced. The results provide important constraints on theoretical models for understanding the mechanism of superconductivity in magic-angle twisted bilayer graphene.

The discovery of superconductivity in magic-angle twisted bilayer graphene (tBLG) has raised intriguing questions about the nature of the superconducting order parameter (*1*–*3*). The phase diagram of magic-angle tBLG, featuring both the correlated insulator (CI) and superconducting phases, resembles that of cuprate materials, suggesting that the superconducting phase arises from an unconventional origin (*1*, *4*–*6*, *7*–*12*). By contrast, the more recent observations of superconductivity in the absence of CI appear to indicate that superconductivity arises through electron-phonon coupling (*13*–*15*), an interpretation that is backed by a range of theoretical models (*16*–*18*).

It has long been recognized that elucidating the role of Coulomb interaction is essential to determining the nature of superconductivity. For a conventional superconductor, electron-phonon coupling competes against Coulomb repulsion in stabilizing superconductivity at low temperature (*19*, *20*). As such, a weaker Coulomb repulsion will lead to more robust superconducting order parameters. By contrast, an unconventional superconducting phase arises from an all-electron mechanism, whereby the order parameter strengthens with increasing Coulomb interaction (*4*, *5*). For conventional solid-state materials, it remains an experimental challenge to directly control Coulomb interaction within a superconductor without introducing additional changes to the material. The flexibility of the van der Waals materials offers a valuable opportunity to control Coulomb interaction in magic-angle tBLG structure using proximity screening (*13*, *14*, *21*).

A major roadblock for addressing the mechanism underlying the superconducting phase is the vastly different behavior across different

[1]Department of Physics, Brown University, Providence, RI 02912, USA. [2]National Institute for Materials Science, 1-1 Namiki, Tsukuba 305-0044, Japan. [3]Department of Physics, Florida State University, Tallahassee, FL 32306, USA. [4]National High Magnetic Field Laboratory, Tallahassee, FL 32310, USA.
*Corresponding author. Email: jia_li@brown.edu

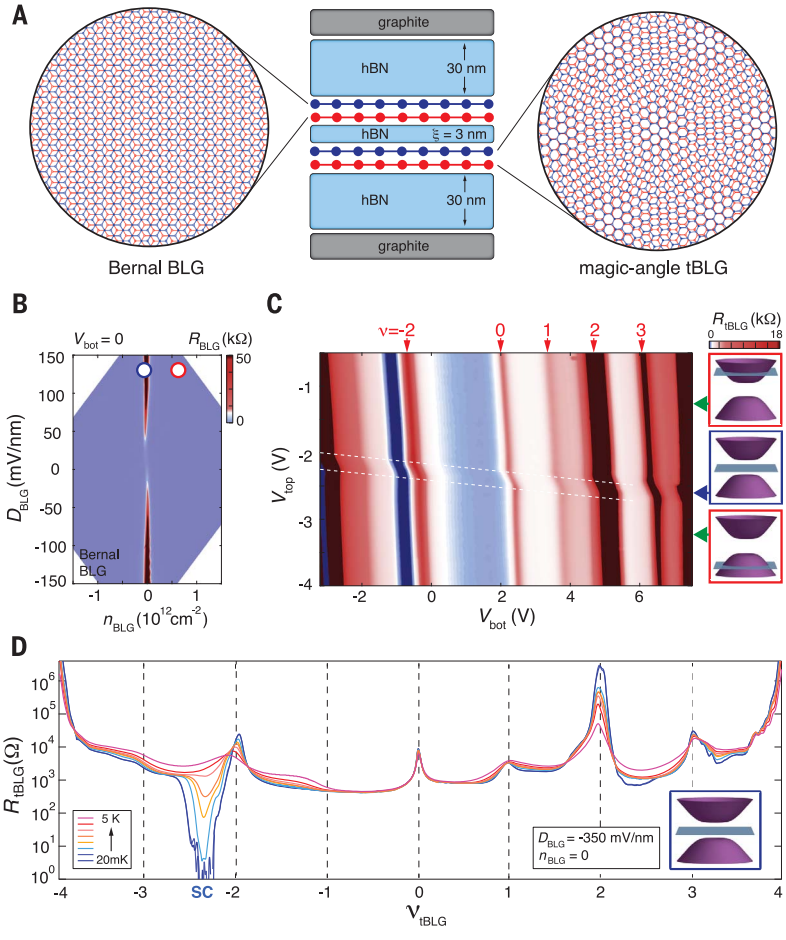

Fig. 1. Hybrid double-layer structure with Bernal BLG and tBLG. (**A**) Schematic of the hybrid double-layer structure consisting of a Bernal BLG and a magic-angle tBLG, separated by a thin insulating barrier with thickness of $\xi = 3$ nm. The structure is encapsulated with dual hexagonal boron nitride (hBN) dielectric and graphite gate electrodes. (**B**) Longitudinal resistance of Bernal BLG R_{BLG} as a function of D_{BLG} and n_{BLG} at $T = 20$ mK. (**C**) Longitudinal resistance of tBLG R_{tBLG} as a function of V_{top} and V_{bot} measured at $T = 20$ mK and $V_{int} = -200$ mV. Screening from BLG is minimal between the white dashed lines, where BLG is fully insulating and tBLG is tuned with both top and bottom graphite gates, giving rise to the distortion in transport features. Inset: Schematic energy structure of BLG at large D_{BLG} for three values of n_{BLG}. (**D**) R_{tBLG} as a function of filling fraction in tBLG ν_{tBLG}, measured at $D_{BLG} = -350$ mV/nm and $n_{BLG} = 0$ with varying temperature.

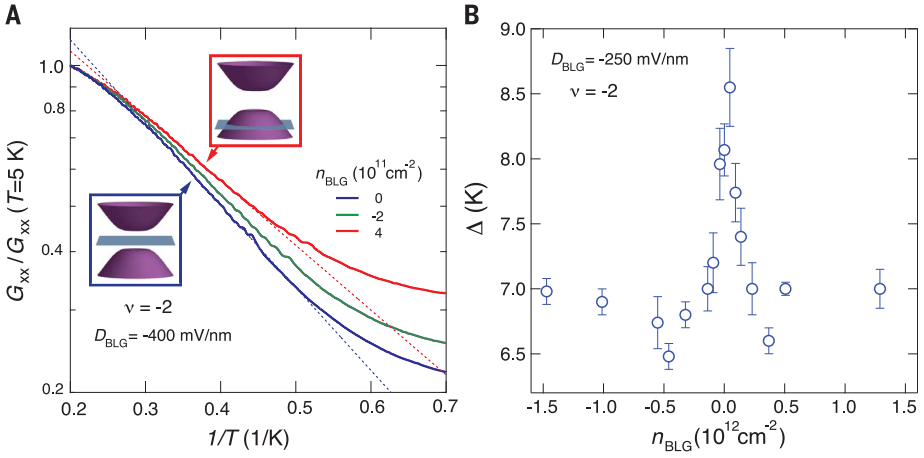

Fig. 2. The effect of Coulomb screening on the CI. (**A**) Arrhenius plot for the correlated insulating state at $\nu_{tBLG} = -2$, measured at $D_{BLG} = -400$ mV/nm with varying carrier density n_{BLG}. Four-terminal conductances G_{xx} measured at different n_{BLG} are normalized by their value at $T = 5$ K. (**B**) Activation energy gap of the $\nu_{tBLG} = -2$ CI state as a function of n_{BLG}.

tBLG samples near the magic angle, which may result from the spatial inhomogeneity of the moiré pattern (*22*–*24*). The variation between different samples makes it difficult to provide reliable experimental constraints on a theoretical model. Here, we address this obstacle by tuning the strength of the Coulomb interaction in a single device using screening, while studying the response in both the CIs and the superconducting phase using transport measurement. We use a hybrid double-layer structure, in which a Bernal bilayer graphene (BLG) and a magic-angle twisted bilayer graphene (tBLG) are separated by a thin insulating barrier with a $\xi = 3$ nm thickness (Fig. 1A). The close proximity allows charge carriers from BLG to screen the Coulomb interaction in the tBLG, offering direct control of electron correlations in the moiré flat band.

Charge carrier density in BLG and tBLG, n_{BLG} and n_{tBLG}, can be independently controlled by varying the applied voltage to the top and bottom graphite gates, V_{top} and V_{bot} (*25*). Additionally, a voltage bias across two layers V_{int} induces a perpendicular electric field, D, providing experimental control for the energy gap at the charge neutrality point in BLG (*26*–*28*). Longitudinal resistance measured from the Bernal BLG displays a well-defined peak at the neutrality point, which grows more insulating with increasing D-field (Fig. 1B). At large D-field, Bernal BLG can be tuned from fully insulating at $n_{BLG} = 0$ (blue circle in Fig. 1B) to highly conductive at large n_{BLG} (red circle in Fig. 1B), offering a large contrast in the strength of Coulomb screening. Figure 1C plots the transport response of tBLG with a twist angle of $\theta = 1.04^o$ (*25*), as n_{BLG} and n_{tBLG} are both tuned by varying V_{top} and V_{bot}. A normalized density scale, marked by red arrows, is defined to describe partial filling ν of the moiré band on the basis of the fourfold degeneracy of spin and valley degrees of freedom for both electron- and hole-type carriers.

The static e^2/r Coulomb interaction among the electrons with charge e, separated by distance r in the tBLG, is modified by the presence of BLG, leading to an effective interaction energy

$$V^{\text{eff}}(r) = \int \frac{d^2q}{(2\pi)^2} \frac{2\pi e^2}{|q|} \left[1 - e^{-2|q|\xi}\left(1 - \frac{1}{\epsilon_{AB}(q)}\right)\right] e^{iq\cdot r}$$

The wave vector q-dependent dielectric constant of the BLG can be related to its static polarization function Π_q^0 as $\epsilon_{AB}(q) = 1 + \frac{2\pi e^2}{|q|}\Pi_q^0$. When the BLG is gated to a finite carrier density and thus acts as a metal, $\Pi_{q\to 0}^0 \to$ const. and the $\epsilon_{AB}(q \to 0)$ diverges. At long distances, $V^{\text{eff}}(r)$ then corresponds to the real space potential produced by the test charge and its mirror image a distance 2ξ above the twisted bilayer. When the BLG is insulating, $\Pi_{q\to 0}^0 \sim q^2$ and the $V^{\text{eff}}(r)$ is unchanged at long distances by the presence of the BLG [see (*25*) for details of Coulomb screening in a hybrid double-layer structure at any r]. Because the strength of Coulomb screening is correlated with the conductivity of BLG, its effect can be studied by comparing transport properties of tBLG in and outside the density range marked by the white dashed lines in Fig. 1C.

First, we examine the transport response of tBLG in the absence of Coulomb screening, by measuring inside the white dashed lines in Fig. 1C, where BLG is fully insulating. Figure 1D plots the longitudinal resistance of tBLG, R_{tBLG}, over the full filling range of the moiré flat band. Apart from the charge neutral point (CNP), a series of resistive features emerge at $\nu = \pm 2, +1$, and $+3$, which are consistent with the CI states from previous observation (*1*–*3*). In addition, a robust superconducting phase emerges at low temperature, evidenced by R_{tBLG} dropping to zero. The robust CI and superconducting states establish an excellent starting point, allowing us to quantitatively examine the effect of Coulomb screening by studying the variation in transport behavior while varying n_{BLG}.

Figure 2A plots the temperature dependence of four-terminal conductance of the CIs at $\nu = -2$, which exhibits thermally activated behavior with strong n_{BLG} dependence. An energy gap Δ can be extracted from the slope of the Arrhenius plot (dashed lines in Fig. 2A), providing a measure for the strength of the CI state. The effect of Coulomb screening is investigated by measuring the energy gap Δ while varying density in BLG n_{BLG} (Fig. 2B). $\Delta_{\nu=-2}$ is largest when BLG is fully insulating at $n_{BLG} = 0$. Similar behavior in the energy gap is observed at $\nu = 2$ and 3 as a function of n_{BLG} [see figs. S11 and S12 (*25*)]. Because CIs at integer fillings arise from Coulomb correlation within the moiré flat band (*6*, *29*, *30*, *31*), the trend in Δ provides strong evidence that electron correlations in tBLG are directly tunable using Coulomb screening: Screening from the BLG decreases as BLG becomes insulating, leading to stronger Coulomb interactions and a larger Δ for the CI states. In addition, a minimum in $\Delta_{\nu=-2}$ is observed near the band edge of BLG at $n_{BLG} \sim 5 \times 10^{11}$ cm^{-2}, suggesting that Coulomb screening is strongest when the Fermi level of BLG is near the van Hove singularities, where the density of states is largest (*32*, *33*). We note that BLG at $n_{BLG} = 0$ remains insulating over the temperature range of the thermal activation measurement, ensuring that the strength of Coulomb screening remains constant with varying temperature and is controlled only by n_{BLG} [see figs. S13 and S14 (*25*)]. The robustness of the CI at $\nu = -2$ in the presence of strong Coulomb screening suggests that CIs cannot be fully suppressed by Coulomb screening alone (*13*). The effect of Coulomb screening on CIs shows excellent agreement with theoretical models (*25*), which provides an important reference for studying the nature of superconductivity in tBLG using Coulomb screening from BLG.

Having established the effect of Coulomb screening on CIs, we turn our attention to the superconducting phase on the hole-doping side of $\nu = -2$. Figure 3A plots R_{tBLG} at $T = 20$ mK as a function of carrier density in tBLG, n_{tBLG}. The superconducting phase is stable over a wider density range in the regime where BLG is metallic (red trace in Fig. 3A), as compared to when BLG is fully insulating (blue trace in Fig. 3A). The boundary of the superconducting region is defined by the density where R_{tBLG}

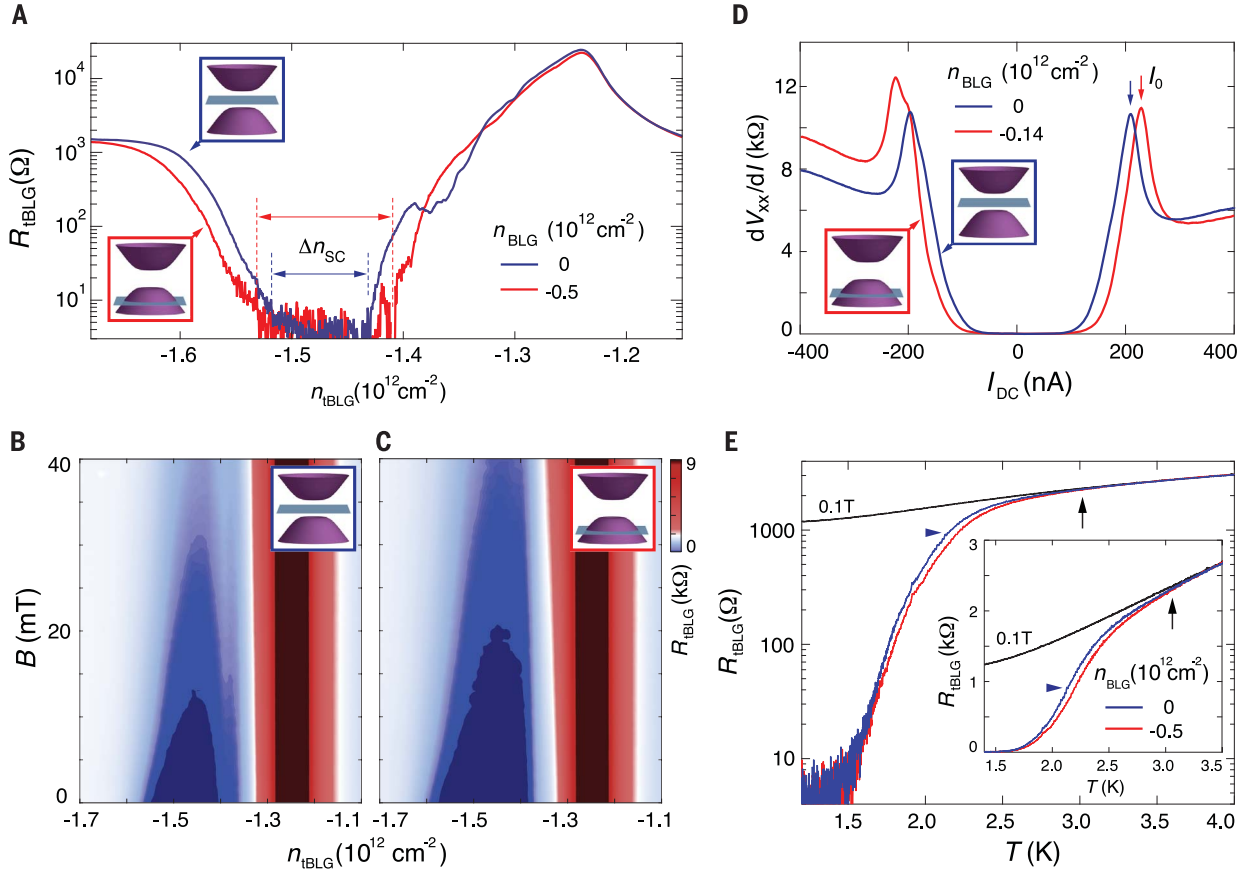

Fig. 3. The effect of tuning n_{BLG} in the presence of a large *D*-field–induced energy gap in BLG. (**A**) R_{tBLG} as a function of carrier density in tBLG, n_{tBLG}, measured at $D_{BLG} = -350$ mV/nm with different n_{tBLG} at $T = 20$ mK. (**B** and **C**) R_{tBLG} as a function of carrier density n_{tBLG} and perpendicular magnetic field B at $T = 20$ mK. BLG is tuned to $D_{BLG} = -350$ mV/nm with (B) $n_{BLG} = 0$ and (C) $n_{BLG} = -0.5 \times 10^{12}$ cm^{-2}. (**D**) Differential resistance dV_{xx}/dI versus d.c. bias current I_{DC} measured at optimal doping $n_{tBLG} = -1.48 \times 10^{12}$ cm^{-2} and base temperature of $T = 20$ mK, with D_{BLG} = 350 mV/nm and BLG tuned to different density. A critical current I_o is defined by the peak in dV_{xx}/dI, where superconductivity is destroyed and the differential resistance goes over to the normal state value (*40*). (**E**) R_{tBLG} as a function of temperature measured at optimal doping $n_{tBLG} = -1.48 \times 10^{12}$ cm^{-2} and $D_{BLG} = -350$ mV/nm for different n_{BLG}. The blue and red traces are measured at $B = 0$, whereas the black trace is measured at the perpendicular magnetic field $B = 0.1$ T where superconductivity is fully suppressed. Inset: Temperature dependence of R_{tBLG} on a linear scale. T_c is operationally defined by 50% of normal state resistance and marked by the blue horizontal arrowhead. The separation of $B = 0$ and $B = 0.1$ T curves marks the onset of pairing (black vertical arrow).

increases above the noise level, which determines the density range of the superconducting dome, Δn_{SC}, as shown in Fig. 3A. The effect of n_{BLG} tuning is also observed in the density-magnetic field phase diagram, where zero resistance is shown as dark blue in the chosen color scale. A larger superconducting region is observed at large n_{BLG} (Fig. 3C) compared with $n_{BLG} = 0$ (Fig. 3B). Figure 3, D and E, respectively, show the measurements of the critical current I_o and critical temperature T_c of the superconducting phase at the optimal doping, which confirm the same trend: The superconducting phase is more robust when BLG is metallic as compared to fully insulating. We note that R_{tBLG} measured at $B = 0.1$ T, where superconductivity is fully suppressed, reflects the transport behavior of tBLG in the normal state. The transition temperature T_c, operationally defined as 50% of extrapolated normal state resistance, is shown to be ~2.2 K in Fig. 3E, which is in line with previous observations in tBLG with a similar twist angle (*14*). The temperature dependence of R_{tBLG} leads to a few important observations: (i) The normal state ($T \gtrsim 3$ K)resistance in tBLG is insensitive to changes in BLG, demonstrating that modifications in impurity scattering resulting from a nearby metallic layer do not play a dominating role (*34*); (ii) the onset of Cooper pairing is observed at $T \sim 3$ K (vertical black arrow in Fig. 3E), evidenced by the bifurcation between R_{tBLG} measured at $B = 0$ and 0.1 T. We note that the n_{BLG}-tuning and Cooper pairing onset at a similar temperature, as shown by the red and blue traces in Fig. 3E. The stability of the superconducting phase can be further explored by plotting I_o, T_c, and Δn_{SC} as a function of n_{BLG}. The values of all three properties closely follow the conductance of BLG, as shown in Fig. 4, A to D, with the superconducting phase at the optimal doping being more robust when BLG is metallic. Taken together, our measurements suggest that n_{BLG} tuning has a direct impact on the stability of the superconducting phase in tBLG.

The enhancement of superconductivity by a nearby metallic BLG layer could, in principle, result from suppressed phase fluctuations in tBLG, without an appreciable effect on Cooper pair formation, giving rise to a higher Berezinskii-Kosterlitz-Thouless transition temperature T_{BKT} (*35*). We can rule out this scenario because the n_{BLG} tuning onsets at roughly the same temperature as Cooper

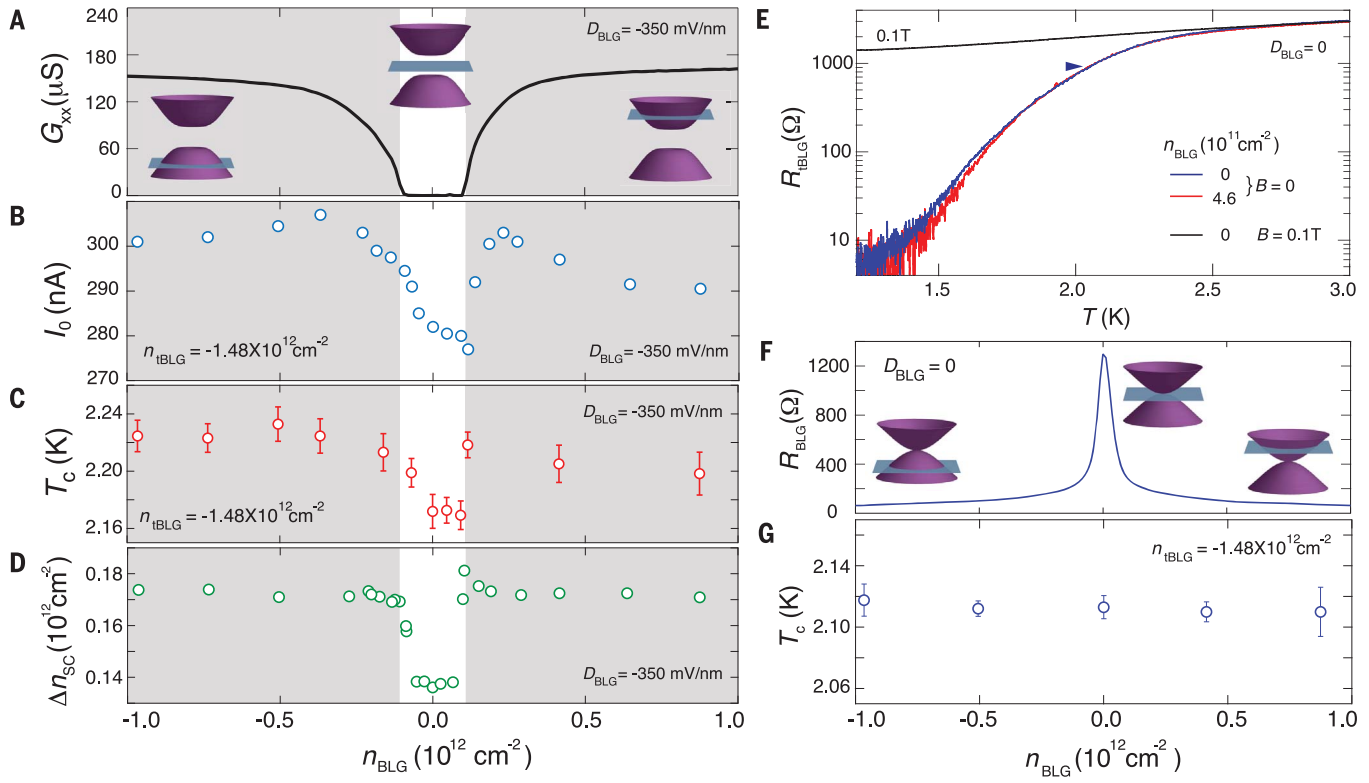

Fig. 4. The effect of tuning n_{BLG} on the superconductivity at the optimal doping in magic-angle tBLG. (**A**)The longitudinal conductance G_{xx} in BLG as a function of carrier density n_{BLG} measured at $D_{BLG} = -350$ mV/nm and $T = 20$ mK. Insets show the position of Fermi level relative to the energy band structure in BLG at different carrier densities. (**B**) I_o, (**C**) T_c, and (**D**) Δn_{SC} as a function of carrier density in BLG, n_{BLG}, measured at $D_{BLG} = -350$ mV/nm. I_o and T_c are measured at optimal doping $n_{tBLG} = -1.48 \times 10^{12}$ cm^{-2}, I_o and Δn_{SC} are measured at $T = 20$ mK. A large energy gap is induced in BLG by D-field. (**E**) R_{tBLG} as a function of temperature measured at optimal doping $n_{tBLG} = -1.48 \times 10^{12}$ cm^{-2} and $D_{BLG} = 0$ for different n_{BLG}. The blue and red traces are measured at $B = 0$, whereas the black trace is measured at $B = 0.1$ T, where superconductivity is fully suppressed. Tuning n_{BLG} gives rise to small differences in R_{tBLG} at temperatures much lower than T_c; no effect is observed in the temperature range near T_c. (**F**) R_{xx} in BLG as a function of carrier density n_{BLG} measured at $D_{BLG} = 0$ and $T = 20$ mK. (**G**) T_c as a function of carrier density in BLG, n_{BLG}, measured at $D_{BLG} = 0$ and optimal doping $n_{tBLG} = -1.48 \times 10^{12}$ cm^{-2}.

pairing (Fig. 3E). Additional support for this conclusion is provided by our data at $D_{BLG} = 0$; in this regime, the gap at the neutrality point of BLG is zero and BLG is always conducting, although the resistivity of BLG varies by about a factor of 20 between the CNP and away from it (Fig. 4F). As a result, tuning n_{BLG} away from the CNP suppresses phase fluctuation in tBLG, which is evidenced by small changes in R_{tBLG} at a temperature much lower than T_c. However, the temperature dependence of R_{tBLG} remained the same on the Cooper pairing scale at $T \sim 2$ K (Fig. 4E), giving rise to a constant value in T_c over a wide range of n_{BLG} (Fig. 4G), indicating that tuning n_{BLG} at $D_{BLG} = 0$ does not change the strength of Coulomb screening.

In addition, we note that in the absence of filtering, the superconducting phase is greatly suppressed when BLG is metallic (*25*). This is possibly due to the influence of radio frequency noise from outside the measurement apparatus (*36*), which is amplified by the capacitive coupling across the insulating barrier in a double-layer structure (*37*). The influence of such external radiation can be eliminated by installing a low-pass filter [see fig. S3 (*25*)]. The enhancement of superconductivity by a nearby metallic layer indicates that the influence of an external high-frequency radiation is sufficiently eliminated by filtering.

It is also worth pointing out that changes in Coulomb screening do not influence the linear-in-T behavior in tBLG at high temperature (fig. S10). It has been suggested that the slope of R_{tBLG} in the T-linear regime is associated with the strength of quasielastic electron scattering off acoustic phonon modes (*38*, *39*). Transport measurement in this regime demonstrates a constant slope of R_{tBLG} independent of carrier density in BLG, n_{BLG} (fig. S10), which would imply that the strength of acoustic electron-phonon coupling is not influenced by Coulomb screening. Our result suggests that the dominant effect of n_{BLG} tuning is changing the strength of Coulomb interactions in the magic-angle tBLG. That Cooper pair formation and superconductivity at the optimal doping become more robust with increasing screening appears consistent with electron-phonon coupling competing against Coulomb interaction to stabilize the superconducting phase (*19*). Alternatively, Coulomb screening could affect superconductivity by modifying properties of the moiré flatband, such as the size of fermi surface. The ability to control Coulomb interaction promises to provide important constraints on theoretical models aiming to accurately describe superconductivity in magic-angle tBLG.

REFERENCES AND NOTES

1. Y. Cao *et al.*, *Nature* **556**, 43–50 (2018).
2. M. Yankowitz *et al.*, *Science* **363**, 1059–1064 (2019).
3. X. Lu *et al.*, *Nature* **574**, 653–657 (2019).
4. B. Keimer, S. A. Kivelson, M. R. Norman, S. Uchida, J. Zaanen, *Nature* **518**, 179–186 (2015).
5. P. A. Lee, N. Nagaosa, X.-G. Wen, *Rev. Mod. Phys.* **78**, 17–85 (2006).
6. Y. Cao *et al.*, *Nature* **556**, 80–84 (2018).
7. Y. Cao *et al.*, *Phys. Rev. Lett.* **124**, 076801 (2020).
8. C. Xu, L. Balents, *Phys. Rev. Lett.* **121**, 087001 (2018).
9. H. Isobe, N. F. Q. Yuan, L. Fu, *Phys. Rev. X* **8**, 041041 (2018).

10. H. Guo, X. Zhu, S. Feng, R. T. Scalettar, *Phys. Rev. B* **97**, 235453 (2018).
11. S. Ray, J. Jung, T. Das, *Phys. Rev. B* **99**, 134515 (2019).
12. D. V. Chichinadze, L. Classen, A. V. Chubukov, *Phys. Rev. B* **101**, 224513 (2020).
13. P. Stepanov *et al*., *Nature* **583**, 375–378 (2020).
14. Y. Saito, J. Ge, K. Watanabe, T. Taniguchi, A. F. Young, *Nat. Phys.* **16**, 926–930 (2020).
15. H. S. Arora *et al*., *Nature* **583**, 379–384 (2020).
16. M. Ochi, M. Koshino, K. Kuroki, *Phys. Rev. B* **98**, 081102 (2018).
17. B. Lian, Z. Wang, B. A. Bernevig, *Phys. Rev. Lett.* **122**, 257002 (2019).
18. F. Wu, A. H. MacDonald, I. Martin, *Phys. Rev. Lett.* **121**, 257001 (2018).
19. W. L. McMillan, *Phys. Rev.* **167**, 331–344 (1968).
20. P. B. Allen, R. C. Dynes, *Phys. Rev. B* **12**, 905–922 (1975).
21. J. M. Pizarro, M. Rösner, R. Thomale, R. Valentí, T. O. Wehling, *Phys. Rev. B* **100**, 161102 (2019).
22. H. Yoo *et al*., *Nat. Mater.* **18**, 448–453 (2019).
23. L. J. McGilly *et al*., arXiv:1912.06629 [cond-mat.mes-hall] (2019).
24. A. Uri *et al*., *Nature* **581**, 47–52 (2020).
25. See the supplementary materials.
26. Y. Zhang *et al*., *Nature* **116**, 136802 (2009).
27. J. I. A. Li *et al*., *Science* **358**, 648–652 (2017).
28. A. A. Zibrov *et al*., *Nature* **549**, 360–364 (2017).
29. R. Bistritzer, A. H. MacDonald, *Proc. Natl. Acad. Sci. U.S.A.* **108**, 12233–12237 (2011).
30. C. Wu, D. Bergman, L. Balents, S. Das Sarma, *Phys. Rev. Lett.* **99**, 070401 (2007).
31. J. Kang, O. Vafek, *Phys. Rev. Lett.* **122**, 246401 (2019).
32. A. F. Young, L. S. Levitov, *Phys. Rev. B Condens. Matter Mater. Phys.* **84**, 085441 (2011).
33. B. M. Hunt *et al*., *Nat. Commun.* **8**, 948 (2017).
34. L. Ponomarenko *et al*., *Nat. Phys.* **7**, 958–961 (2011).
35. L. Merchant, J. Ostrick, R. P. Barber, R. C. Dynes, *Phys. Rev. B Condens. Matter Mater. Phys.* **63**, 134508 (2001).
36. I. Tamir *et al*., *Sci. Adv.* **5**, eaau3826 (2019).
37. M. J. Kellogg, Evidence for excitonic superfluidity in a bilayer two-dimensional electron system, Ph.D. thesis, California Institute of Technology (2005).
38. F. Wu, E. Hwang, S. Das Sarma, *Phys. Rev. B* **99**, 165112 (2019).
39. H. Polshyn *et al*., *Nat. Phys.* **15**, 1011–1016 (2019).
40. A. Benyamini *et al*., *Nat. Phys.* **15**, 947–953 (2019).
41. X. Liu *et al*., Data repository for: Tuning electron correlation in magic-angle twisted bilayer graphene using Coulomb screening, Version 1.0, Open Science Framework (2020). https://osf.io/uewx4/?view only=d112e55af9bc46f294a7fea4c087248d

ACKNOWLEDGMENTS

We thank M. Yankowitz, A. F. Young, C. R. Dean, Q. Shi, S. Todadri, and S. A. Kivelson for discussions and Y. Zeng for helpful input on fabrication. **Funding:** This work was primarily supported by Brown University. Device fabrication was performed in the Institute for Molecular and Nanoscale Innovation at Brown University. The authors acknowledge the use of equipment funded by the MRI award DMR-1827453. O.V. was supported by NSF DMR-1916958, and by the National High Magnetic Field Laboratory through NSF grant no. DMR-1157490 and the State of Florida. K.W. and T.T. acknowledge support from the EMEXT Element Strategy Initiative to Form Core Research Center through grant no. JPMXP0112101001 and the CREST(JPMJCR15F3), JST. **Author contributions:** X.L. and Z.W. fabricated the device and performed the measurements. X.L., Z.W., and J.I.A.L. analyzed the data. O.V. constructed the theoretical model. K.W. and T.T. provided the hBN crystals. The manuscript was written with input from all authors. **Competing interests:** The authors declare no competing financial interests. **Data and materials availability:** Experimental data files are available at the Open Science Framework (*41*)

SUPPLEMENTARY MATERIALS

science.sciencemag.org/content/371/6535/1261/suppl/DC1
Materials and Methods
Supplementary Text
Figs. S1 to S15
References (*42*–*44*)

24 March 2020; accepted 8 February 2021
10.1126/science.abb8754

Science

Tuning electron correlation in magic-angle twisted bilayer graphene using Coulomb screening

Xiaoxue Liu, Zhi Wang, K. Watanabe, T. Taniguchi, Oskar Vafek and J. I. A. Li

Science **371** (6535), 1261-1265.
DOI: 10.1126/science.abb8754

Tuning the interactions

Elucidating the nature of the superconducting state in magic-angle twisted bilayer graphene (MATBG) has proven tricky. To study the role of electron-electron correlations in this state, Liu *et al.* placed another graphene bilayer, this one having a conventional arrangement of the graphene sheets, in the immediate vicinity of a sample of MATBG. By varying the carrier density in the conventional bilayer, the researchers controlled the strength of interactions in MATBG. Weakening the interactions strengthened superconductivity, consistent with scenarios in which the electron-phonon coupling competes against Coulomb interactions to stabilize the superconducting phase.

Science, this issue p. 1261

Science (print ISSN 0036-8075; online ISSN 1095-9203) is published by the American Association for the Advancement of Science, 1200 New York Avenue NW, Washington, DC 20005. The title *Science* is a registered trademark of AAAS.